Exploring the Chemical Dynamics of Phenanthrene ($C_{14}H_{10}$) Formation via the Bimolecular Gas-Phase Reaction of the Phenylethynyl Radical (C_6H_5CC) with Benzene (C_6H_6)

Authors and Affiliations: Shane J. Goettl[a], Zhenghai Yang[a], Chao He[a], Ankit Somani[b], Adrian Portela-Gonzalez[b], Wolfram Sander[b]*, Alexander M. Mebel[c]*, Ralf I. Kaiser[a]*

[a] Department of Chemistry, University of Hawaii at Manoa, Honolulu, Hawaii 96822, USA
Email: ralfk@hawaii.edu

[b] Lehrstuhl für Organische Chemie II, Ruhr-Universität Bochum, 44801 Bochum, Germany
Email: wolfram.sander@rub.de

[c] Department of Chemistry and Biochemistry, Florida International University, Miami, Florida 33199, USA
Email: mebela@fiu.edu

Abstract

The exploration of the fundamental formation mechanisms of polycyclic aromatic hydrocarbons (PAHs) is crucial for the understanding of molecular mass growth processes leading to two- and three-dimensional carbonaceous nanostructures (nanosheets, graphenes, nanotubes, buckyballs) in extraterrestrial environments (circumstellar envelopes, planetary nebulae, molecular clouds) and combustion systems. While key studies have been conducted exploiting traditional, high-temperature mechanisms such as the hydrogen abstraction–acetylene addition (HACA) and phenyl addition–dehydrocyclization (PAC) pathways, the complexity of extreme environments highlights the necessity of investigating chemically diverse mass growth reaction mechanisms leading to PAHs. Employing the crossed molecular beams technique coupled with electronic structure calculations, we report on the gas-phase synthesis of phenanthrene ($C_{14}H_{10}$)—a three-ring, 14π benzenoid PAH—via a phenylethynyl addition–cyclization–aromatization mechanism, featuring bimolecular reactions of the phenylethynyl radical (C_6H_5CC, X^2A_1) with benzene (C_6H_6) under single collision conditions. The dynamics involve a phenylethynyl radical addition to benzene without entrance barrier leading eventually to phenanthrene via indirect scattering dynamics through $C_{14}H_{11}$ intermediates. The barrierless nature of reaction allows rapid access to phenanthrene in low-temperature environments such as cold molecular clouds which can reach temperatures as low as 10 K. This mechanism constitutes a unique, low-temperature framework for the formation of PAHs as building blocks in molecular mass growth processes to carbonaceous nanostructures in extraterrestrial environments thus affording critical insight into the low-temperature hydrocarbon chemistry in our universe.

Keywords: Gas-Phase Reactions, Polycyclic Aromatic Hydrocarbons, Reaction Mechanisms, Radical Intermediates, Low Temperature

Introduction

Polycyclic aromatic hydrocarbons (PAHs)—organic molecules consisting of fused six- membered rings with delocalized π-electrons—have drawn substantial interest from the combustion science and astrochemistry communities due to their vital role as reactive intermediates and molecular building blocks of carbonaceous nanomaterials in the form of soot along with circumstellar and interstellar grains.[1-5] In deep space, PAHs have been suspected to account for up to 30 % of the cosmic carbon budget and are implicated as carriers of diffuse interstellar bands (DIBs)[6] and unidentified infrared (UIR) bands.[7] Sophisticated analyses of carbonaceous chondrites such as Allende[8] and Murchison[9] revealed the presence of PAHs synthesized in circumstellar envelopes of carbon-rich asymptotic giant branch (AGB) stars and planetary nebulae as their descendants.[10] Functionalized PAHs 1- and 2-cyanonaphthalene[11] as well as 2-cyanoindene[12] have recently been observed via spectral line surveys of the Taurus Molecular Cloud (TMC-1). However, astrochemical models predict the lifetimes of PAHs in the interstellar medium (ISM) to be on the order of 10^8 years, whereas the timescale for formation and injection of PAHs from carbon stars to the ISM has been derived to be on the order of 10^9 years.[13] This discord indicates an incomplete understanding of their fundamental formation mechanisms and suggests previously uncharted routes to PAHs in deep space.

To this end, unconventional reaction mechanisms and mass growth processes involving formerly overlooked reactants must be searched in order to fully comprehend PAH evolution in extreme environments. Previous molecular beam experiments coupled with electronic structure calculations exposed exotic spiroaromatic intermediates[14] and unconventional excited state dynamics[15] leading to PAHs such as anthracene ($C_{14}H_{10}$) thus highlighting 'non-traditional' gas-phase routes to multi-ringed aromatics. Considering the inclusion of an aromatic ring, the phenylethynyl radical (C_6H_5CC, X^2A_1) constitutes a promising candidate as a precursor in bottom-up PAH synthesis. This radical presents the opportunity for a much larger mass growth step than those in traditional formation mechanisms such as hydrogen abstraction – acetylene addition (HACA) [16] and hydrogen abstraction – vinylacetylene addition (HAVA)[17] which involve multiple steps to account for observed PAH abundances in interstellar environments and combustion flames.[18] In these high temperature circumstellar environments, phenylethynyl radicals can be accessed through hydrogen abstraction from phenylacetylene (C_6H_5CCH), which has been observed in the ISM,[19,20] while the barrierless bimolecular reaction of dicarbon with benzene—

both species ubiquitous in extreme environments—produces the phenylethynyl radical even in cold molecular clouds at temperature as low as 10 K.[21] Hence, reactions of phenylethynyl radicals with prevalent unsaturated hydrocarbons constitute promising pathways toward the formation of PAHs. However, only studies on phenylethynyl radical reactions with allene (H_2CCCH_2) and methylacetylene (CH_3CCH) have explored the reaction dynamics of the phenylethynyl radical experimentally thus far. While these reactions demonstrated the high, barrierless reactivity of the phenylethynyl radical with unsaturated hydrocarbons, only addition–elimination pathways without cyclization were observed.[22] Moreover, reactions of the 1-propynyl (CH_3CC, X^2A_1) radical—where the phenyl group is replaced by a methyl group—with small hydrocarbons, such as acetylene (C_2H_2),[23] ethylene (C_2H_4),[24] methylacetylene (CH_3CCH),[25] 1,3-butadiene (C_4H_6),[26] and benzene (C_6H_6),[27] result in addition–elimination pathways along with cyclization involving only the ethynyl group, leaving the methyl moiety as a spectator throughout. The exception is the 1-propynyl reaction with allene (H_2CCCH_2) which also produces the benzene isomer fulvene (C_6H_6), though the dynamics show distinct non-RRKM behavior.[25] By replacing the methyl group with a conjugated π system as with the phenylethynyl radical, we hope to initiate cyclization and aromatization involving the benzene moiety as a new route toward the formation of PAHs in extreme environments.

Herein, we report on the bimolecular, gas-phase reaction of the phenylethynyl radical (C_6H_5CC, X^2A_1) with benzene-*d*$_6$ (C_6D_6) under single-collision conditions by exploiting the crossed molecular beams technique. Combining the experimental results with electronic structure calculations reveals pathways to the formation of phenanthrene-*d*$_6$ ($C_{14}H_4D_6$) coupled with atomic hydrogen loss. The reaction proceeds through a phenylethynyl addition–cyclization–aromatization channel featuring barrierless addition of the radical center of the phenylethynyl radical to benzene-*d*$_6$ forming long-lived intermediates undergoing multiple hydrogen migration and ring opening/closing isomerization steps before unimolecular decomposition via atomic hydrogen loss in an overall exoergic process. This mechanism, due to its barrierless nature, opens up these reactions in cold environments such as dense molecular clouds where temperatures are as low as 10 K[28] and serves as a non-traditional route toward the low-temperature formation of PAHs eventually leading to complex carbonaceous nanostructures providing insight on the interstellar evolution of carbon in our galaxy.

Methods

Experimental

The reaction of the phenylethynyl radical (C_6H_5CC, X^2A_1) with benzene-d_6 (C_6D_6, 99.96 % D atom, Sigma Aldrich) was conducted under single-collision conditions using a crossed molecular beams machine.[29] The (2-bromoethynyl)benzene (C_6H_5CCBr) precursor was purified in a stainless steel bubbler by multiple freeze–pump–thaw cycles and seeded at a fraction of 0.5 % in two carrier gases, helium (He, 99.9999 %, Matheson) and neon (Ne, 99.9999 %, Matheson), to vary the collision energy. The precursor gas mixture was held at a backing pressure of 500 Torr before exiting a Proch-Trickl[30] pulsed valve with a 120 Hz repetition rate, −450 V amplitude, and open time of 80 μs. The molecular beam was intersected by an excimer laser (Coherent, COMPex 110) operating at 193 nm, 60 Hz, and 10 mJ per pulse thus generating phenylethynyl radicals *in situ* via photodissociation of (2-bromoethynyl)benzene.[22] The molecular beam was then skimmed, and a chopper wheel selected a portion of the beam with a velocity (v_p) of 1745 ± 14 m s^{-1} and speed ratio (S) of 9.4 ± 0.8 for the helium-seeded case and a v_p of 896 ± 6 m s^{-1} and S of 13.9 ± 0.8 for the neon-seeded case. The phenylethynyl beam crossed perpendicularly with a pulsed benzene-d_6 (10 % in He, v_p = 1110 ± 25 m s^{-1}, S = 23.3 ± 0.5) beam with a backing pressure of 550 Torr and pulsed valve parameters of −400 V and 120 Hz. This resulted in collision energies (E_C) of 98.1 ± 2.4 and 46.7 ± 1.5 kJ mol^{-1}, as well as center-of-mass (CM) angles (Θ_{CM}) of 28.6 ± 0.8 and 46.6 ± 0.8°, for the helium-seeded and neon-seeded systems, respectively (Table 1).

Table 1. Peak velocities (v_p) and speed ratios (S) for the phenylethynyl radical (C_6H_5CC) and benzene-d_6 (C_6D_6) beams as well as the corresponding collision energies (E_c) and center-of-mass angles (Θ_{CM}) for each reactive scattering experiment.

Beam	v_p (m s^{-1})	S	E_c (kJ mol^{-1})	Θ_{CM} (°)
C_6D_6 (X^1A_{1g})	1110 ± 25	23.3 ± 0.5		
C_6H_5CC (X^2A_1) / He	1745 ± 14	9.4 ± 0.8	98.1 ± 2.4	28.6 ± 0.8
C_6H_5CC (X^2A_1) / Ne	896 ± 6	13.9 ± 0.8	46.7 ± 1.5	46.6 ± 0.8

Products formed through reactive scattering were identified via a triply differentially pumped mass spectrometric detector, which is rotatable in the plane of the reactant beams. In the ionizer region, this system can be pumped down to high 10^{-13} Torr range. The neutral products were ionized by electron impact ionization at 80 eV and filtered by a quadrupole mass spectrometer (150QC, Extrel) operating in the time-of-flight (TOF) mode. Up to 1.4×10^6 TOFs were taken at each angle in either 2.5° steps in the $21.8° \leq \Theta \leq 52.3°$ angular range with 0° defined by the phenylethynyl beam. A laboratory angular distribution (LAD) was derived by integrating the TOFs at different angles and normalizing to Θ_{CM}. To obtain additional chemical dynamics information on the system, the laboratory data were fit using a forward convolution routine, in which user-defined CM translational energy ($P(E_T)$) and angular ($T(\theta)$) flux distributions were refined iteratively until a reasonable fit of the data was achieved.[31,32] Assuming separability of the product speed and angular distributions, the CM flux contour map is then defined as $I(u,\theta) \approx P(u) \times T(\theta)$, where the product velocity in the CM frame is determined from E_T.[33]

Computational

Geometries of various species involved in the reaction of the phenylethynyl radical with benzene, such as $C_{14}H_{11}$ intermediates and transition states, the reactants, and $C_{14}H_{10}$ products, were optimized at the hybrid density functional ωB97XD level of theory[34] with the 6-311G(d,p) basis set. Vibrational frequencies and zero-point vibrational energies (ZPE) were obtained using the same ωB97XD/6-311G(d,p) approach. Single-point energies at the optimized geometries of all species were then refined employing the G3(MP2,CC)//B3LYP modification[35,36] of the original Gaussian 3 (G3) scheme.[37] The final energies at 0 K were obtained including ωB97XD ZPE corrections according to the following formula:

$$E_0[G3(MP2,CC)] = E[CCSD(T)/6\text{-}311G(d,p)] + \Delta E_{MP2} + E(ZPE)$$

where $\Delta E_{MP2} = E[MP2/G3large] - E[MP2/6\text{-}311G(d,p)]$ is the basis set correction and E(ZPE) is the zero-point energy. In order to minimize spin contamination, restricted open-shell calculations for the radical species were carried out both at the MP2 (ROMP2) and CCSD(T) (ROCCSD(T)) levels using the initial ROHF wavefunctions. The electronic structure calculations were carried out employing the Gaussian 16[38] and MOLPRO 2021[39] quantum chemistry packages.

Next, the energetic and molecular parameters from the electronic structure calculations were utilized using the Rice−Ramsperger−Kassel−Marcus (RRKM) theory[40] to compute energy-dependent rate constants for all unimolecular reaction steps taking place on the $C_{14}H_{11}$ PES following the initial $C_6H_5CC + C_6D_6$ association step. In these calculations, the internal energy for each $C_{14}H_{11}$ intermediate or transition state was set as a sum of the collision and chemical activation energies, with the chemical activation energy being a negative of the energy of the species relative to the initial reactants. The rate constants calculations were performed at the zero-pressure limit, with the aim to reproduce the crossed molecular beams conditions. Finally, the RRKM-computed rate constants were used in calculations of reaction product branching ratios within the steady-state approximation.[41]

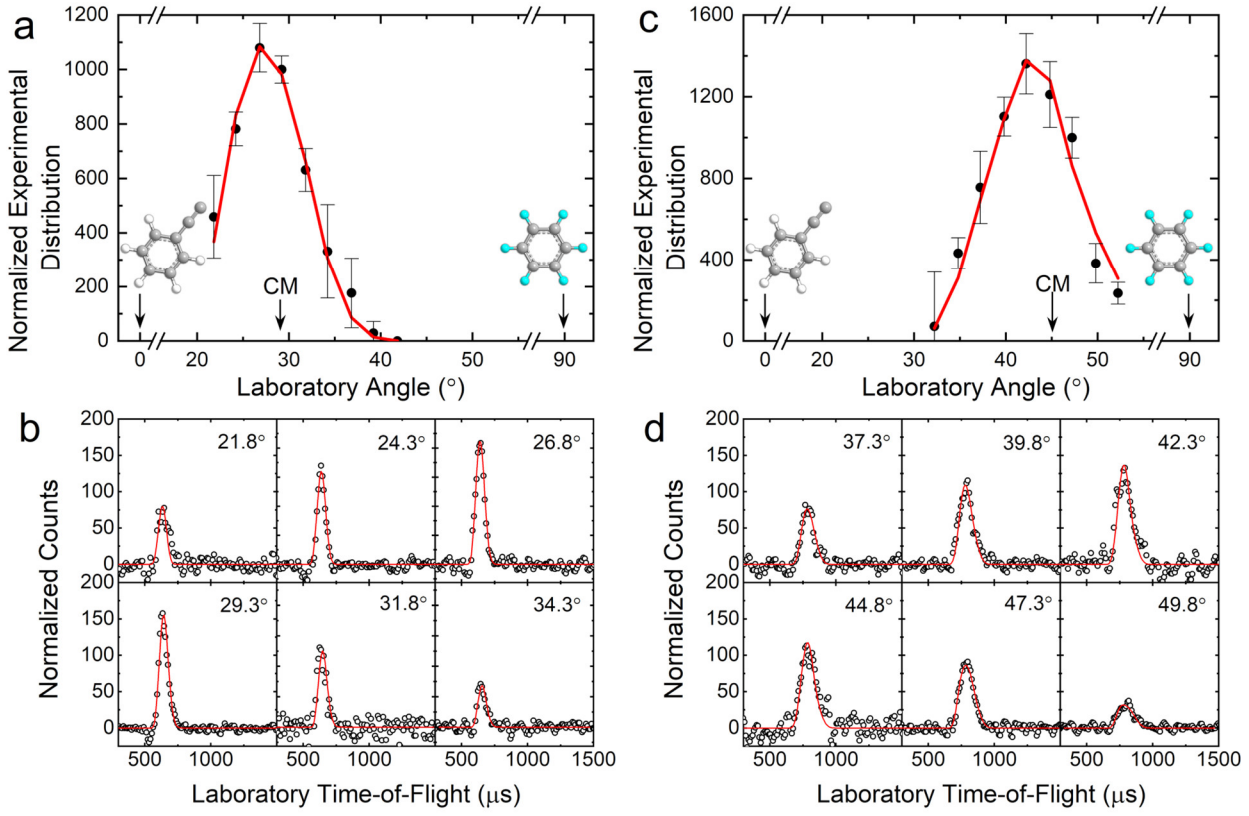

Fig. 1 Laboratory angular distributions (**a, c**) and time-of-flight (TOF) spectra (**b, d**) recorded at mass-to-charge (m/z) = 184 for the reaction of phenylethynyl (C_6H_5CC) with benzene-d_6 (C_6D_6) conducted at collision energies of 98.1 ± 2.4 kJ mol^{-1} (**a, b**) and 46.7 ± 1.5 kJ mol^{-1} (**c, d**). CM represents the center-of-mass angle, and 0° and 90° define the directions of the phenylethynyl and benzene-d_6 beams, respectively. The black circles depict the data and red lines the fits. Carbon atoms are colored gray, hydrogens are white, and deuterium atoms are light blue.

Results

Laboratory Frame

For the reaction of the phenylethynyl radical with benzene-d_6, reactive scattering data (Fig. 1) were collected for both high (E_C = 98.1 ± 2.4 kJ mol^{-1}) and low (E_C = 46.7 ± 1.5 kJ mol^{-1}) collision energies at a mass-to-charge ratio (m/z) of 184 ($C_{14}H_4D_6^+$) indicating the formation of $C_{14}H_4D_6$ isomer(s) coupled with atomic hydrogen loss. There was no signal observed for the adduct at m/z = 185 and background intensity prevented any measurement of m/z = 183. The TOFs at high collision energies (Fig. 1b) were fairly narrow and only about 200 μs wide, while at low collision energies (Fig. 1d) the TOFs were broadened to about 300 μs. The LADs in both cases feature a slight asymmetry about Θ_{CM} toward the primary (phenylethynyl) beam (Figs. 1a and 1c). While strong forward or backward peaking in the LAD suggests direct scattering dynamics, the slight asymmetry suggests indirect reaction mechanism(s) through $C_{14}H_5D_6$ intermediate(s). Since the benzene-d_6 reactant is fully deuterated, the observed H loss indicates that the hydrogen atom emission originates from the phenylethynyl reactant (Reaction (1)).

$$C_6H_5CC\ (101\ amu) + C_6D_6\ (84\ amu) \rightarrow C_{14}H_4D_6\ (184\ amu) + H\ (1\ amu) \quad (1a)$$

$$\rightarrow C_{14}H_5D_5\ (183\ amu) + D\ (2\ amu) \quad (1b)$$

Center-of-Mass Frame

With the detection of $C_{14}H_4D_6$ isomer(s) plus atomic hydrogen in the reaction of phenylethynyl with benzene-d_6, we now attempt to acquire critical information of the nature of the intermediates and products along with the overall reaction dynamics. This is accomplished by transforming the laboratory data to the CM reference frame. At both collision energies, the data could be fit with a single reaction channel corresponding to 184 amu ($C_{14}H_4D_6$) plus 1 amu (H). Turning first to the $P(E_T)$ (Figs. 2a and 2d), the maximum product kinetic energy release (E_{max}) is 439 ± 59 and 401 ± 50 kJ mol^{-1} for high and low collision energies, respectively. Utilizing the conservation of energy for those products without internal excitation, $\Delta_r G = E_C - E_{max}$, the reaction energy ($\Delta_r G$) can be recovered as −341 ± 61 kJ mol^{-1} (high E_C) and −354 ± 52 kJ mol^{-1} (low E_C). In addition, the $P(E_T)$s feature a distribution maximum at 123 and 96 kJ mol^{-1}, respectively. This reveals that the reaction pathways have exit channels with tight transition states involving substantial electron density rearrangement leading to $C_{14}H_4D_6$ products.[42] The angular flux distributions show intensity over the full angular range, reinforcing the implication of indirect scattering dynamics (Figs. 2b and 2e). The $T(\theta)$ also display a fair amount of forward asymmetry with an intensity ratio $I(0°)/I(180°)$ of about (1.7 ± 0.3):1.0 and (3.5 ± 0.5):1.0 for high and low collision energies, respectively, which

suggests the existence of at least one channel where complex formation takes place but the lifetime is too short to allow multiple rotations (osculating complex).[43] The findings for both collision energies are reflected in the flux contour maps (Figs. 2c and 2f).

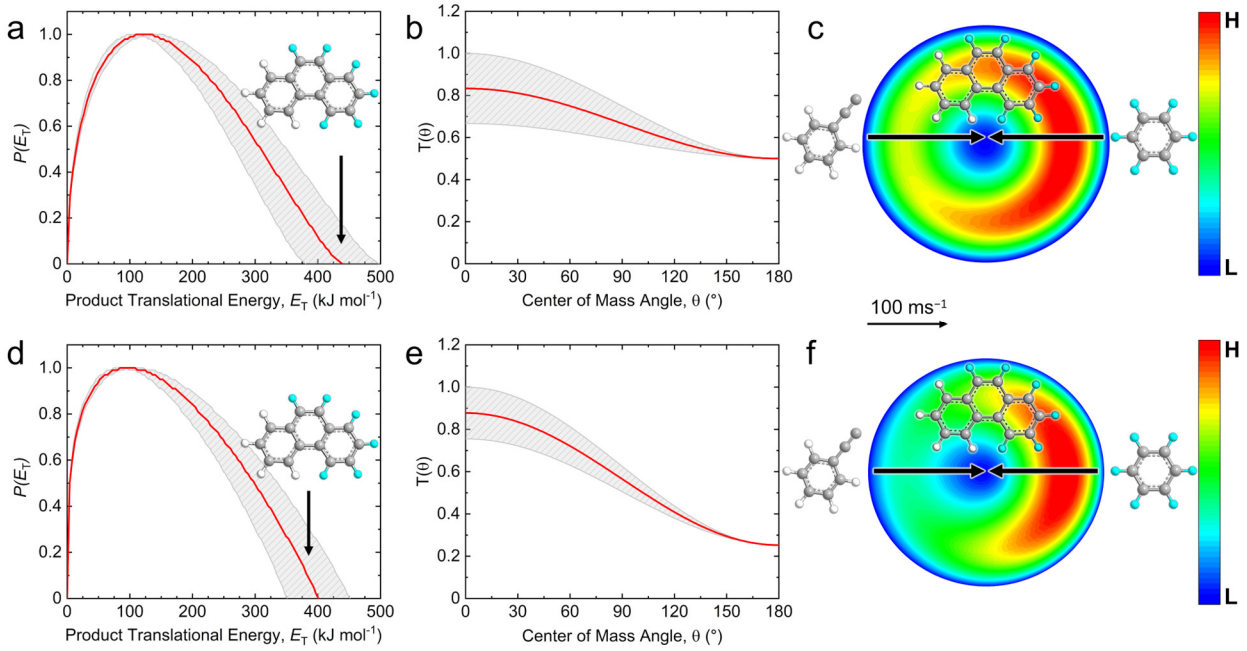

Fig. 2 CM product translational energy (**a, d**) and angular (**b, e**) flux distributions, as well as the associated flux contour maps (**c, f**) leading to the formation of $C_{14}H_4D_6$ product(s) in the reaction of phenylethynyl (C_6H_5CC) with benzene-d_6 (C_6D_6) conducted at collision energies of 98.1 ± 2.4 kJ mol^{-1} (**a–c**) and 46.7 ± 1.5 kJ mol^{-1} (**d–f**). Red lines define the best-fit functions while shaded areas provide the error limits. The flux contour map represents the intensity of the reactively scattered products as a function of product velocity (u) and scattering angle (θ), and the color bar indicates flux gradient from high (H) to low (L) intensity.

Discussion

To reveal the underlying reaction mechanism(s), the experimental findings were merged with electronic structure calculations. The potential energy surfaces (PES) are shown in Figs. 3 and 4, where the latter indicates the positions of the deuterium atoms for the benzene-d_6 case. The experimentally derived reaction energies of −341 ± 61 and −354 ± 52 kJ mol^{-1} for high and low collision energies, respectively, match the calculated reaction energy of −340 ± 8 kJ mol^{-1} for the formation of phenanthrene (**p1**, $C_{14}H_{10}$) in the reaction of the phenylethynyl radical with benzene

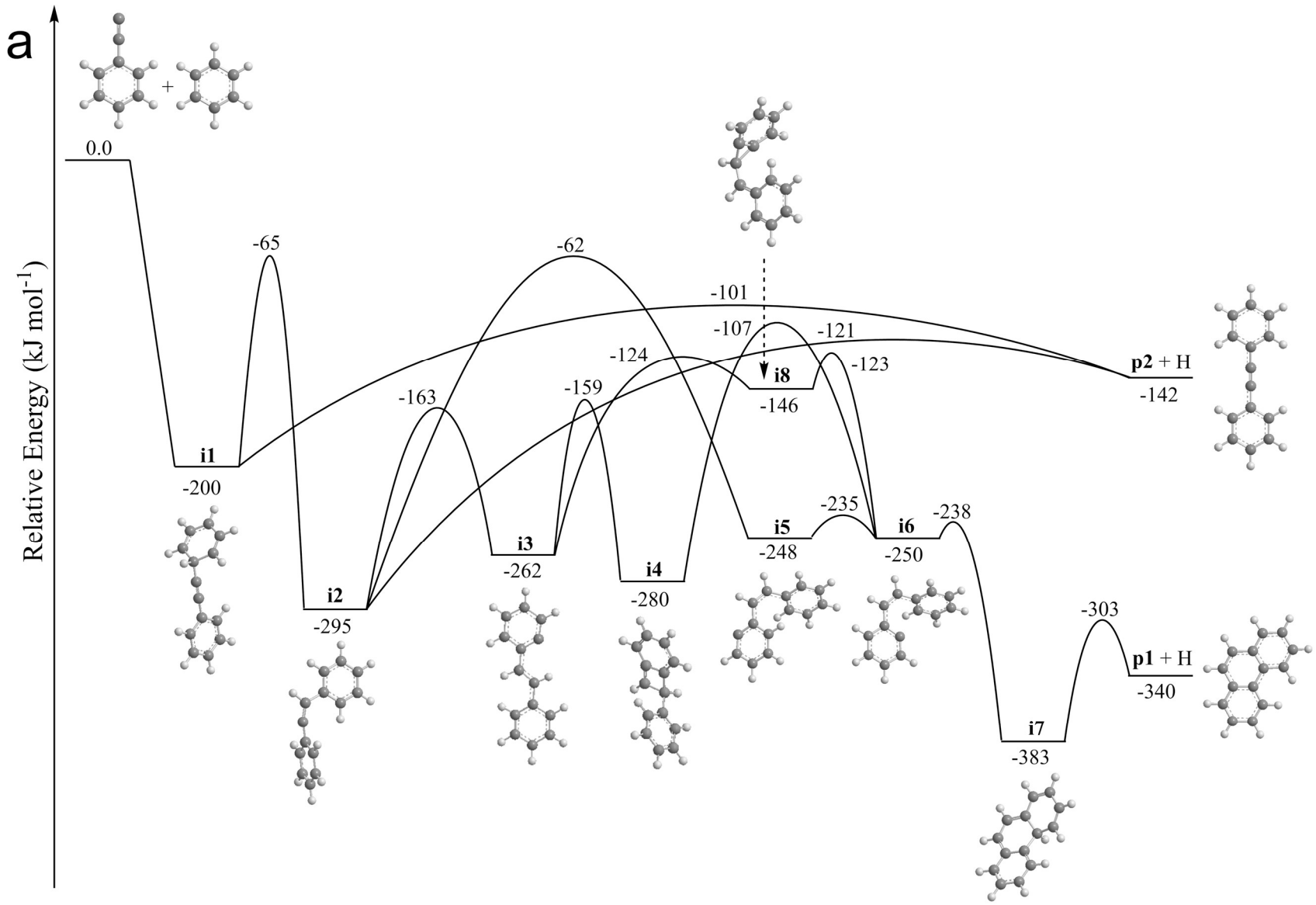
a
Relative Energy (kJ mol-1)
0.0
-65
-62
-101
-107
-121
-124
-123
-163
-159
-146
-142
p2 + H
i1
-200
i2
-295
i3
-262
i4
-280
i5
-248
i6
-250
-235
-238
i7
-383
-303
p1 + H
-340
i8

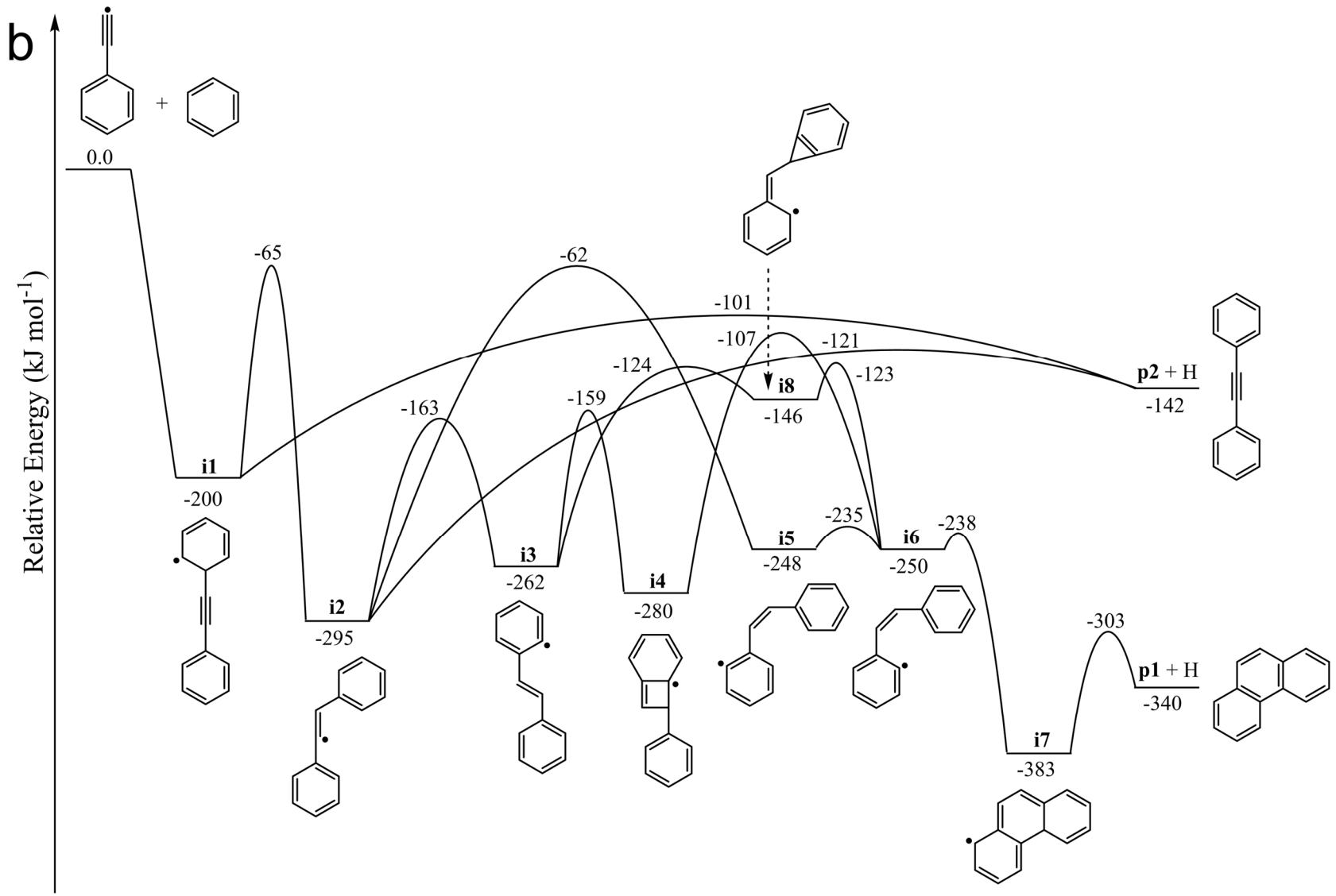

Fig. 3 Calculated potential energy surface for the reaction of phenylethynyl (C_6H_5CC) with benzene (C_6H_6) at the G3(MP2,CC)//ωB97XD/6-311G(d,p) level showing 3D (**a**) and 2D (**b**) structures.

exceptionally well. While diphenylacetylene (**p2**, −142 kJ mol^{-1}) lies much higher in energy than the experimentally observed values, it cannot be discounted on the energetics alone since products with a smaller kinetic energy release can be veiled within the lower energy portion of the $P(E_T)$.

The reaction is initiated by a barrierless addition of the radical center on the terminal carbon of the ethynyl moiety of the phenylethynyl radical to one of the carbons of benzene forming the collision complex **i1**. This intermediate is located 200 kJ mol^{-1} below the separated reactants. From here, hydrogen atom ejection may ensue over a 99 kJ mol^{-1} barrier to form diphenylacetylene (**p2**) in an overall exoergic reaction (−142 ± 8 kJ mol^{-1}). Alternatively, a [1,2] hydrogen shift from **i1** over a 135 kJ mol^{-1} barrier leads to **i2**; this process involved a hydrogen atom shift from the benzene moiety (C1 atom) to the ethynyl bridge. There is one additional pathway to **p2** which involved unimolecular decomposition of **i2** through a tight exit transition state located 21 kJ mol^{-1} above the separated products. Intermediate **i2** can also isomerize via a large barrier of 233 kJ mol^{-1} to **i5** through [1,3] hydrogen shift. This time, the migrating hydrogen atom originates from the benzene moiety of the phenylethynyl radical reactant. This is followed by rotation around a single C-C bond through a low lying transition state to **i6**. The two benzene moieties connect then via ring closure to a six-membered ring over a small barrier of 12 kJ mol^{-1} to **i7** before unimolecular decomposition to phenanthrene via hydrogen atom loss via a tight exit transition state 37 kJ mol^{-1} above **p1**. Finally, **i2** can undergo a [1,4] hydrogen shift from the attacked benzene moiety forming **i3** via a 132 kJ mol^{-1} barrier, which is followed by a ring closure (**i3** → **i4**) to a four-membered ring and reopening (**i4** → **i6**) through 103 and 173 kJ mol^{-1} barriers or a three-member ring closure (**i3** → **i8**) and reopening (**i8** → **i6**) through 138 and 23 kJ mol^{-1} barriers, respectively. The pathway via **i8** is slightly more favorable than via **i4** because the highest in energy transition state for the former resides 17 kJ mol^{-1} lower than that for the latter. The remaining steps from **i6** to **p1** remain the same as previously discussed.

Since reactive scattering experiments were conducted with fully deuterated benzene and signal was detected for the atomic hydrogen loss channel (H loss originates from the phenylethynyl reactant), some of the pathways in Fig. 3 can be excluded when a comparison with experiment is made. Fig. 4 shows the PES with benzene replaced by benzene-d_6, where all routes are equivalent to the non-deuterated PES with the only difference being the position of the deuterium atoms. It should be noted that the relative energies for all species which depend on ZPE change very slightly, with exceptions being the products **p1** and **p2** and H/D loss transitions states. Here, the initial

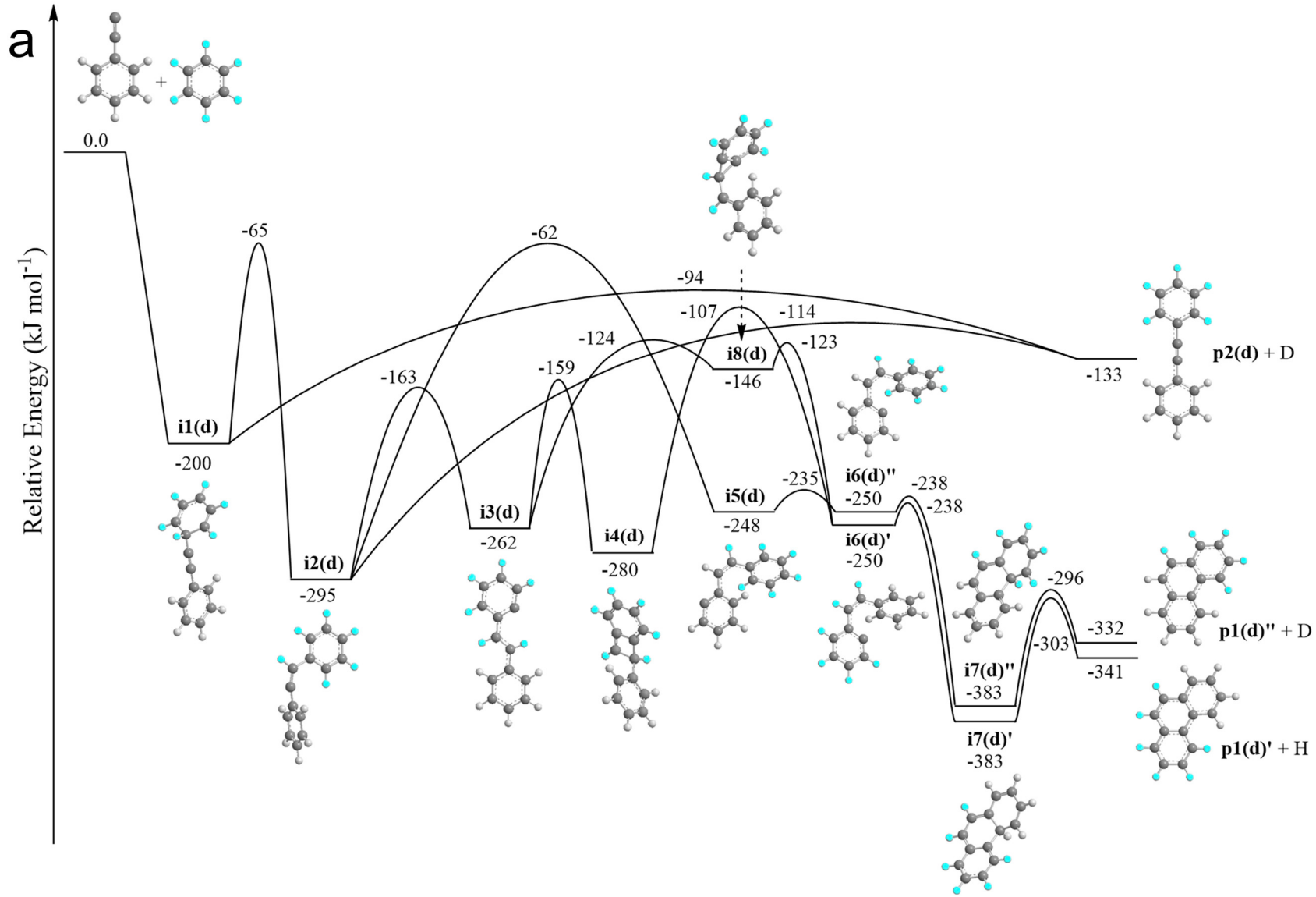
a
Relative Energy (kJ mol-1)
0.0
-65
-62
-94
-107
-114
-123
-124
-159
-163
-133
-200
-295
-262
-280
-146
-248
-235
-250
-238
-238
-250
-296
-303
-332
-341
-383
-383
i1(d)
i2(d)
i3(d)
i4(d)
i8(d)
i5(d)
i6(d)''
i6(d)'
i7(d)''
i7(d)'
p2(d) + D
p1(d)'' + D
p1(d)' + H

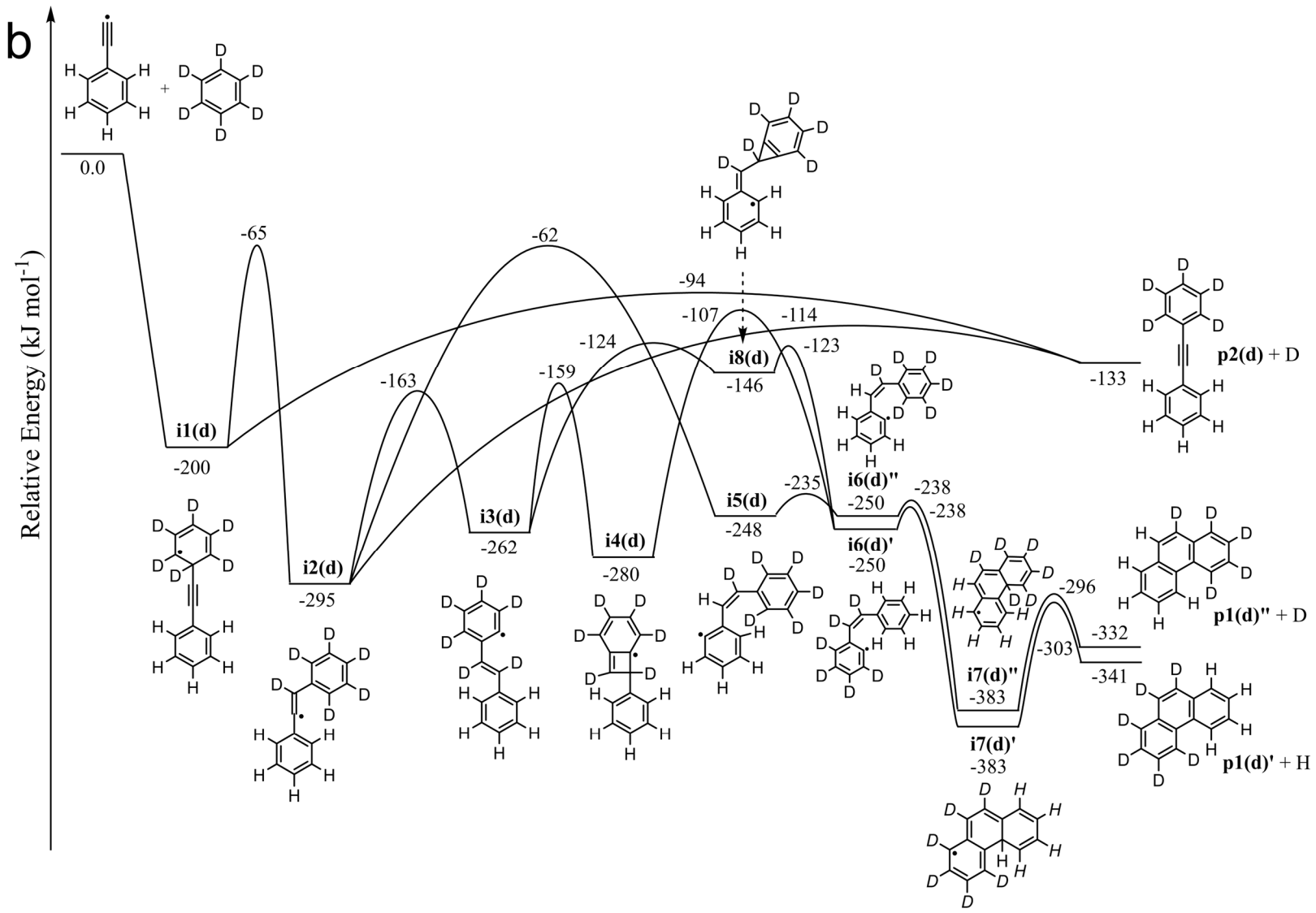

Fig. 4 Potential energy surface for the reaction of phenylethynyl (C_6H_5CC) with benzene-d_6 (C_6D_6) showcasing the positions of the deuterium atoms in 3D (**a**) and 2D (**b**) structures.

collision complex **i1(d)** and intermediate **i2(d)** both lead to diphenylacetylene-d_5 (**p2(d)**) through atomic deuterium loss. These are the only two pathways to **p2(d)**, and there is no atomic hydrogen loss equivalent to **p2** on the PES involving the reaction with deuterated benzene; therefore, diphenylacetylene (**p2** / **p2(d)**) cannot account for the experimentally observed atomic hydrogen loss pathway. Next, **i2(d)** may isomerize to **i5(d)** through a [1,3] H shift and then to **i6(d)″** via bond rotation. At this point, the radical center resides on the non-deuterated benzene ring; thus, cyclization to **i7(d)″** results in a deuterium atom weakly bound to an sp^3 carbon, which is ejected during the formation of product **p1(d)″**. Since this route also leads to atomic deuterium loss, it cannot account for the experimental data. The final pathway involves a deuterium shift (**i2(d)** → **i3(d)**), four-/three-membered ring closure (**i3(d)** → **i4(d)/i8(d)**), and ring opening to **i6(d)′** where the radical center is on the deuterated benzene ring. After closure to a six-membered ring at **i7(d)′**, a hydrogen atom is ejected forming phenanthrene-d_6 (**p1(d)′**). Contrary to the earlier pathways, this route still results in atomic hydrogen loss if the benzene reactant is fully deuterated, thus offering a viable reaction mechanism leading to a product (**p1** / **p1(d)′**) matching the experimentally derived reaction energy.

Considering the energies of the transition states involved in the formation of **p1** and **p2**, the pathways to **p1** should be less favorable than the addition–elimination route to **p2**. This is the consequence of the lower energy transition state connecting the initial collision complex **i1** to **p2** (−101 kJ mol^{-1}) while the rate limiting step to eventually form **p1** requires isomerization of **i1** to **i2** via a barrier higher by 36 kJ mol^{-1} compared to **i1** → **p2**. Consequently, Rice–Ramsperger–Kassel–Marcus (RRKM) statistical calculations predict a product branching ratio of less than 1 % for **p1** indicating that the route to **p2** should dominate. If we increase the critical barrier **i1** → **p2** by 8 kJ mol^{-1} within the anticipated margins of error for relative energies, while decreasing the **i1** → **i2** barrier also by 8 kJ mol^{-1}, the yield of **p1** may rise to 0.8%. While the reaction might be non-statistical, dynamical factors usually favor direct addition-elimination channels and thus are not expected to be favorable for the formation of phenanthrene. Therefore, an alternative explanation needs to be sought to explain the agreement with the RRKM results. Considering the high background counts at m/z = 183, we were unable to scan for the atomic deuterium loss products. So, it is possible that diphenylacetylene-d_5 (**p2(d)**) is formed, but we just cannot detect it. Likewise, the reaction of the phenylethynyl radical with non-deuterated benzene would result in H loss products detected at m/z = 178, which also would be masked by strong background signal. Previous

molecular beam studies showcased formation of products predicted to have very low yields, such as in the reaction of the cyano radical (CN) with dimethylacetylene (CH_3CCCH_3).[44] In that case, the reaction led to the formation of 1-cyano-1-methylallene ($CNCH_3CCCH_2$) coupled with atomic hydrogen loss even though RRKM calculations predicted this channel to account for less than 1 % of the products. The methyl loss pathway was expected to be greater than 99 %, but signal could not be observed for this channel due to interferences from reactive scattering of dimethylacetylene with atomic carbon, which was also in the primary reactant beam.

Conclusion

In summary, our combined experimental and computational investigation revealed that at least phenanthrene-*d*$_6$ ($C_{14}H_4D_6$, **p1(d)′**), coupled with atomic hydrogen loss, was formed under single collision conditions via the bimolecular, gas-phase reaction of the phenylethynyl radical (C_6H_5CC, X^2A_1) with benzene-*d*$_6$ (C_6D_6). The entrance channel involves barrierless addition of the radical center of phenylethynyl to the π-electron system of benzene-*d*$_6$ at one of the equivalent carbons. The ensuing reaction mechanism comprises deuterium migration as well as facile ring opening and closing isomerization steps before unimolecular decomposition of the reaction intermediates to **p1(d)′** through a tight exit transition state via atomic hydrogen loss. The deuterium atom emission route from the initial collision complex **i1(d)** to diphenylacetylene-*d*$_5$ (**p2(d)**) was not observed. This barrierless and exoergic phenylethynyl addition–cyclization–aromatization mechanism represents a unique, low-temperature framework for the synthesis of peri-fused PAHs as building blocks of carbonaceous nanostructures in molecular mass growth processes in deep space. Our observations can be compared to that of the reaction of phenyl radical with phenylacetylene (C_6H_5CCH) which was previously studied both theoretically and experimentally.[45-48] In particular, in the reaction of the phenyl-*d*$_5$ radical (C_6D_5) with phenylacetylene (C_6H_5CCH), where the radical center is located on the unsubstituted reactant (Fig. 5)[46], the experiments revealed the formation of 2-, 3-, and 4-ethynylbiphenyl-*d*$_5$ ($C_{14}H_5D_5$) isomers, while the cyclization to phenanthrene-*d*$_5$ was not detected. This was in line with the RRKM and branching ratio calculations predicting predominant formation of 2-ethynylbiphenyl-*d*$_5$. These divergent findings stress the importance of the location of the radical center on the ensuing reaction mechanism and product formation, while also highlighting the complexity involved in simulating possible reactions toward PAHs in extreme environments.

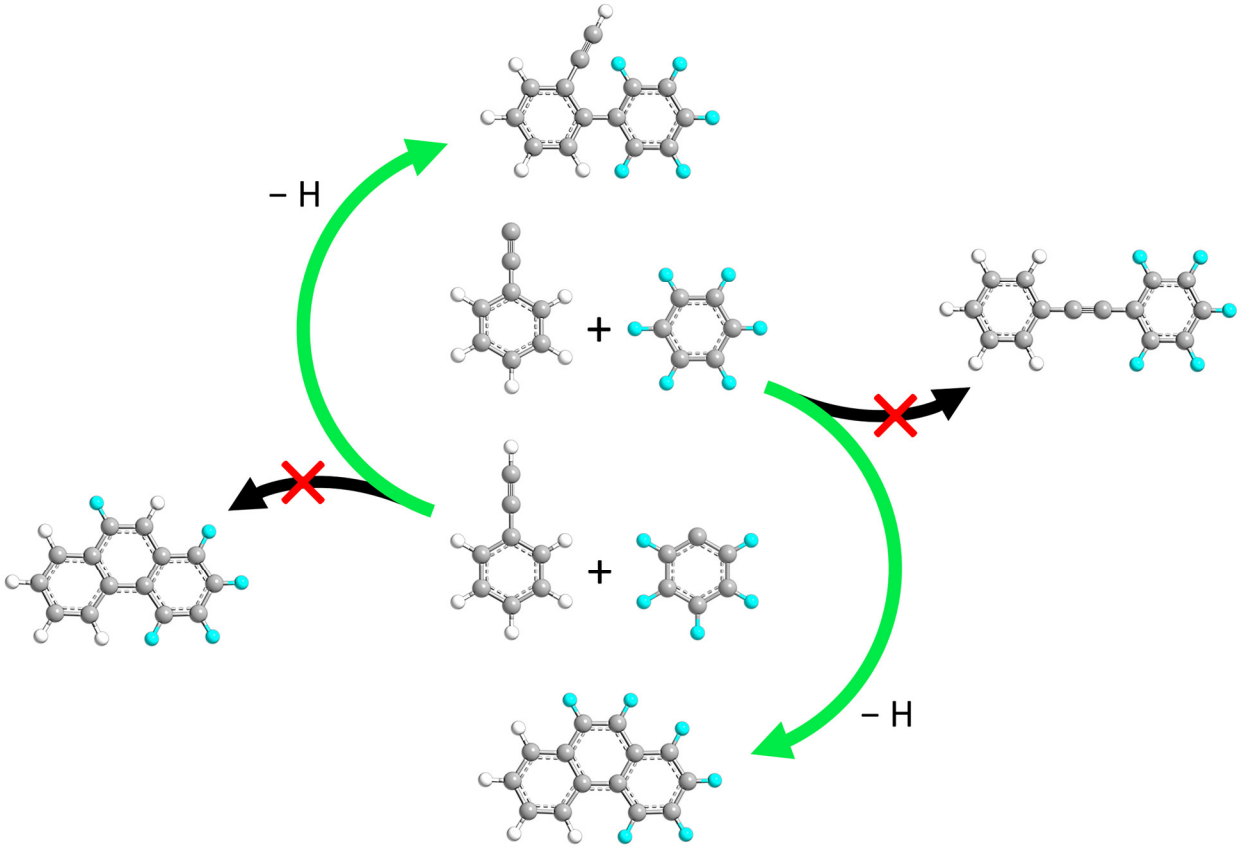

Fig. 5 Main product channels for the reactions of phenylethynyl (C_6H_5CC) with benzene-d_6 (C_6D_6) and phenyl-d_5 (C_6D_5) with phenylacetylene (C_6H_5CCH). Carbon atoms are gray, hydrogen atoms are white, and deuterium atoms are light blue.

Conflicts of Interest

There are no conflicts to declare.

Acknowledgments

The experimental studies at the University of Hawaii were supported by the US Department of Energy, Basic Energy Sciences DE-FG02-03ER15411. The electronic structure and kinetic calculations at the Florida International University were funded by the US Department of Energy, Basic Energy Sciences DE-FG02-04ER15570. The chemical synthesis in Bochum was supported by the Deutsche Forschungsgemeinschaft (DFG, German Research Foundation) under Germany's Excellence Strategy-EXC-2033 390677874 RESOLV.

References

1 E. Reizer, B. Viskolcz and B. Fiser, *Chemosphere*, 2022, **291**, 132793.

2 A. G. G. M. Tielens, in *Dust and Chemistry in Astronomy*, eds. D. A. Williams and T. J. Millar, Institute of Physics Publishing, Bristol, UK, 1993, pp. 99-136.

3 S. Schlemmer, T. Giesen, H. Mutschke and C. Jäger, *Laboratory Astrochemistry: From Molecules through Nanoparticles to Grains*, Wiley-VCH, Singapore, 2014.

4 P. Ehrenfreund and S. B. Charnley, *Annu. Rev. Astron. Astrophys.*, 2000, **38**, 427-483.

5 A. G. G. M. Tielens, *Annu. Rev. Astron. Astrophys.*, 2008, **46**, 289-337.

6 W. W. Duley, *Faraday Discuss.*, 2006, **133**, 415-425.

7 A. M. Ricks, G. E. Douberly and M. A. Duncan, *Astrophys. J.*, 2009, **702**, 301.

8 L. Becker and T. E. Bunch, *Meteorit. Planet. Sci.*, 1997, **32**, 479-487.

9 M. S. de Vries, K. Reihs, H. R. Wendt, W. G. Golden, H. E. Hunziker, R. Fleming, E. Peterson and S. Chang, *Geochim. Cosmochim. Acta*, 1993, **57**, 933-938.

10 F. L. Plows, J. E. Elsila, R. N. Zare and P. R. Buseck, *Geochim. Cosmochim. Acta*, 2003, **67**, 1429-1436.

11 B. A. McGuire, R. A. Loomis, A. M. Burkhardt, K. L. K. Lee, C. N. Shingledecker, S. B. Charnley, I. R. Cooke, M. A. Cordiner, E. Herbst and S. Kalenskii, *Science*, 2021, **371**, 1265-1269.

12 M. L. Sita, P. B. Changala, C. Xue, A. M. Burkhardt, C. N. Shingledecker, K. L. Kelvin Lee, R. A. Loomis, E. Momjian, M. A. Siebert, D. Gupta, E. Herbst, A. J. Remijan, M. C. McCarthy, I. R. Cooke and B. A. McGuire, *Astrophys. J., Lett.*, 2022, **938**, L12.

13 E. R. Micelotta, A. P. Jones and A. G. G. M. Tielens, *Astron. Astrophys.*, 2010, **510**, A36.

14 C. He, R. I. Kaiser, W. Lu, M. Ahmed, Y. Reyes, S. F. Wnuk and A. M. Mebel, *J. Am. Chem. Soc.*, 2023, **145**, 3084-3091.

15 R. Kaiser, L. Zhao, W. Lu, M. Ahmed, V. S. Krasnoukhov, V. N. Azyazov and A. M. Mebel, *Nat. Commun.*, 2022, **13**, 1-8.

16 H. Richter, W. J. Grieco and J. B. Howard, *Combust. Flame*, 1999, **119**, 1-22.

17 D. S. N. Parker, F. Zhang, Y. S. Kim, R. I. Kaiser, A. Landera, V. V. Kislov, A. M. Mebel and A. G. G. M. Tielens, *Proc. Natl. Acad. Sci. U. S. A.*, 2012, **109**, 53-58.

18 H. Jin, A. Frassoldati, Y. Wang, X. Zhang, M. Zeng, Y. Li, F. Qi, A. Cuoci and T. Faravelli, *Combust. Flame*, 2015, **162**, 1692-1711.

19 J. Cernicharo, M. Agúndez, C. Cabezas, B. Tercero, N. Marcelino, J. R. Pardo and P. de Vicente, *Astron. Astrophys.*, 2021, **649**, L15.

20 D. Loru, C. Cabezas, J. Cernicharo, M. Schnell and A. L. Steber, *Astron. Astrophys.*, 2023, **677**, A166.

21 X. Gu, Y. Guo, F. Zhang, A. M. Mebel and R. I. Kaiser, *Chem. Phys. Lett.*, 2007, **436**, 7-14.

22 S. J. Goettl, Z. Yang, S. Kollotzek, D. Paul, R. I. Kaiser, A. Somani, A. Portela-Gonzalez, W. Sander, A. A. Nikolayev, V. N. Azyazov and A. M. Mebel, *J. Phys. Chem. A*, 2023, **127**, 5723-5733.

23 A. M. Thomas, L. Zhao, C. He, A. M. Mebel and R. I. Kaiser, *J. Phys. Chem. A*, 2018, **122**, 6663-6672.

24 C. He, L. Zhao, A. M. Thomas, G. R. Galimova, A. M. Mebel and R. I. Kaiser, *Phys. Chem. Chem. Phys.*, 2019, **21**, 22308-22319.

25 C. He, L. Zhao, A. M. Thomas, A. N. Morozov, A. M. Mebel and R. I. Kaiser, *J. Phys. Chem. A*, 2019, **123**, 5446-5462.

26 A. M. Thomas, C. He, L. Zhao, G. R. Galimova, A. M. Mebel and R. I. Kaiser, *J. Phys. Chem. A*, 2019, **123**, 4104-4118.

27 A. M. Thomas, S. Doddipatla, R. I. Kaiser, G. R. Galimova and A. M. Mebel, *Sci. Rep.*, 2019, **9**, 17595.

28 S. T. Megeath, E. Allgaier, E. Young, T. Allen, J. L. Pipher and T. L. Wilson, *Astron. J.*, 2009, **137**, 4072.
29 X. Gu, Y. Guo and R. I. Kaiser, *Int. J. Mass Spectrom.*, 2005, **246**, 29-34.
30 D. Proch and T. Trickl, *Rev. Sci. Instrum.*, 1989, **60**, 713-716.
31 M. F. Vernon, Ph.D. Dissertation, University of California at Berkeley, 1983.
32 P. S. Weiss, Ph.D. Dissertation, University of California at Berkeley, 1985.
33 R. I. Kaiser, *Chem. Rev.*, 2002, **102**, 1309-1358.
34 J.-D. Chai and M. Head-Gordon, *Phys. Chem. Chem. Phys.*, 2008, **10**, 6615-6620.
35 A. G. Baboul, L. A. Curtiss, P. C. Redfern and K. Raghavachari, *J. Chem. Phys.*, 1999, **110**, 7650-7657.
36 L. A. Curtiss, K. Raghavachari, P. C. Redfern, A. G. Baboul and J. A. Pople, *Chem. Phys. Lett.*, 1999, **314**, 101-107.
37 L. A. Curtiss, K. Raghavachari, P. C. Redfern, V. Rassolov and J. A. Pople, *J. Chem. Phys.*, 1998, **109**, 7764-7776.
38 M. J. Frisch, G. W. Trucks, H. B. Schlegel, G. E. Scuseria, M. A. Robb, J. R. Cheeseman, G. Scalmani, V. Barone, G. A. Petersson, H. Nakatsuji, X. Li, M. Caricato, A. V. Marenich, J. Bloino, B. G. Janesko, R. Gomperts, B. Mennucci, H. P. Hratchian, J. V. Ortiz, A. F. Izmaylov, J. L. Sonnenberg, Williams, F. Ding, F. Lipparini, F. Egidi, J. Goings, B. Peng, A. Petrone, T. Henderson, D. Ranasinghe, V. G. Zakrzewski, J. Gao, N. Rega, G. Zheng, W. Liang, M. Hada, M. Ehara, K. Toyota, R. Fukuda, J. Hasegawa, M. Ishida, T. Nakajima, Y. Honda, O. Kitao, H. Nakai, T. Vreven, K. Throssell, J. A. Montgomery Jr., J. E. Peralta, F. Ogliaro, M. J. Bearpark, J. J. Heyd, E. N. Brothers, K. N. Kudin, V. N. Staroverov, T. A. Keith, R. Kobayashi, J. Normand, K. Raghavachari, A. P. Rendell, J. C. Burant, S. S. Iyengar, J. Tomasi, M. Cossi, J. M. Millam, M. Klene, C. Adamo, R. Cammi, J. W. Ochterski, R. L. Martin, K. Morokuma, O. Farkas, J. B. Foresman and D. J. Fox, *Gaussian 16*, Revision C.01; Gaussian, Inc.: Wallingford, CT, 2016; see http://www.gaussian.com.
39 H. J. Werner, P. J. Knowles, G. Knizia, F. R. Manby, M. Schütz, P. Celani, W. Györffy, D. Kats, T. Korona, R. Lindh, A. Mitrushenkov, G. Rauhut, K. R. Shamasundar, T. B. Adler, R. D. Amos, A. Bernhardsson, A. Berning, D. L. Cooper, J. O. Deegan, A. J. Dobbyn, F. Eckert, E. Goll, C. Hampel, A. Hesselmann, G. Hetzer, T. Hrenar, G. Jansen, C. Köppl, Y. Liu, A. W. Lloyd, R. A. Mata, A. J. May, S. J. McNicholas, W. Meyer, M. E. Mura, A. Nicklass, D. P. O'Neill, P. Palmieri, D. Peng, K. Pflüger, R. Pitzer, M. Reiher, T. Shiozaki, H. Stoll, A. J. Stone, R. Tarroni, T. Thorsteinsson, M. Wang and M. Welborn, *Molpro, a Package of Ab Initio Programs*, Version 2021.2; University of Cardiff: Cardiff, UK, 2021; see http://www.molpro.net.
40 J. I. Steinfeld, J. S. Francisco and W. L. Hase, *Chemical Kinetics and Dynamics*, Prentice Hall, Upper Saddle River, NJ, 2nd edn., 1999.
41 V. V. Kislov, T. L. Nguyen, A. M. Mebel, S. H. Lin and S. C. Smith, *J. Chem. Phys.*, 2004, **120**, 7008-7017.
42 J. Laskin and C. Lifshitz, *Journal of Mass Spectrometry*, 2001, **36**, 459-478.
43 W. B. Miller, S. A. Safron and D. R. Herschbach, *Discuss. Faraday Soc.*, 1967, **44**, 108-122.
44 N. Balucani, O. Asvany, A. Chang, S. Lin, Y. Lee, R. Kaiser, H. Bettinger, P. v. R. Schleyer and H. Schaefer III, *J. Chem. Phys.*, 1999, **111**, 7472-7479.
45 J. Aguilera-Iparraguirre and W. Klopper, *J. Chem. Theory Comput.*, 2007, **3**, 139-145.
46 D. S. N. Parker, T. Yang, R. I. Kaiser, A. Landera and A. M. Mebel, *Chem. Phys. Lett.*, 2014, **595**, 230-236.
47 L. B. Tuli and A. M. Mebel, *International Journal of Chemical Kinetics*, 2020, **52**, 875-883.
48 H. Jin, W. Chen, L. Ye, H. Lou, Q. Xu, B. Feng, Z. Wang and A. Farooq, *Combust. Flame*, 2022, **243**, 112014.